IEEE Photonics Journal
An IEEE Photonics Society Publication

Open Access

Photonic Multiple Microwave Frequency Measurement Based on Frequency-to-Time Mapping

Volume 10, Number 2, April 2018

Feng Zhou
Hao Chen
Xu Wang
Linjie Zhou
Jianji Dong
Xinliang Zhang

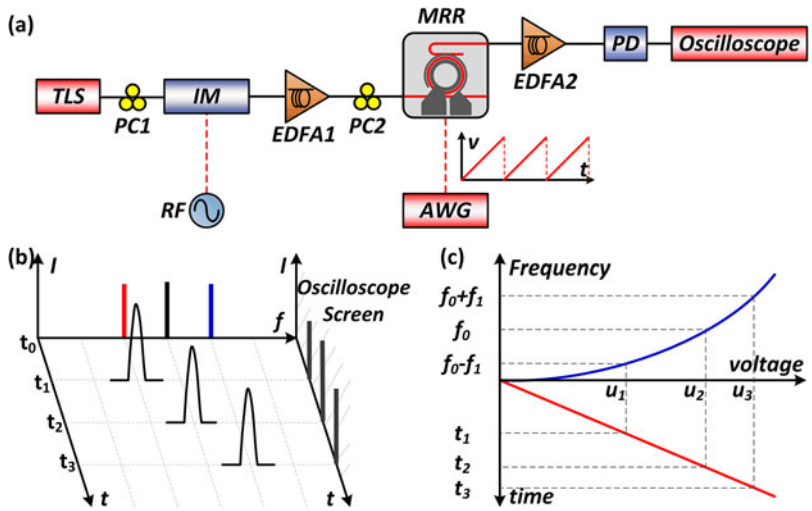

DOI: 10.1109/JPHOT.2018.2807919
1943-0655 © 2018 IEEE

IEEE photonics SOCIETY

IEEE

Photonic Multiple Microwave Frequency Measurement Based on Frequency-to-Time Mapping

Feng Zhou,[1] Hao Chen,[1] Xu Wang,[1] Linjie Zhou,[2] Jianji Dong,[1] and Xinliang Zhang[1]

[1]Wuhan National Laboratory for Optoelectronics, School of Optical and Electronic Information, Huazhong University of Science and Technology, Wuhan 430074, China
[2]State Key Laboratory of Advanced Optical Communication Systems and Networks, Department of Electronic Engineering, Shanghai Jiao Tong University, Shanghai 430074, China

DOI:10.1109/JPHOT.2018.2807919

Manuscript received January 6, 2018; revised February 12, 2018; accepted February 15, 2018. Date of publication February 20, 2018; date of current version March 6, 2018. This work was supported in part by the National Natural Science Foundation of China under Grant 61475052 and Grant 61622502 and in part by the Opened Fund of the State Key Laboratory on Advanced Optical Communication System and Network under Grant 2015GZKF03004. Feng Zhou and Hao Chen contributed equally to this work.
Corresponding author: J. Dong (e-mail: jjdong@mail.hust.edu.cn).

Abstract: A photonic multiple microwave frequency measurement system is presented and demonstrated based on a swept frequency silicon microring resonator (MRR). The drop-port of a high-Q MRR is employed as a periodic narrowband scanning filter driven by a sawtooth voltage signal. The unknown frequency can be mapped to time interval between pulse appearances when scanning the modulated signal and the frequency-to-time mapping is established. In the experiments, we obtain a measurement range of 25 GHz with an error of $\pm$510 MHz. Meanwhile, the measurement resolution for multi-frequency measurement is about 5 GHz. Our scheme offers a simple structure, low-cost solution, capability of multiple frequency measurement, and potential of chip-integration.

Index Terms: Microwave frequency measurement, microwave photonics.

1. Introduction

Recently, microwave frequency measurement (MFM) technique has aroused lots of research interests for its application on electronic warfare, radar warning and electronic intelligence systems. Due to the explosive growth of data traffic, critical challenges are bringing urgent demands to measurements in terms of large instantaneous bandwidth greater than 10 GHz, which may not be achievable using purely electronic solutions or the systems are extremely complicated and costly [1]. Compared with electronics solutions, photonic MFM systems offer advantages including large instantaneous bandwidth, electromagnetic immunity, potential for multi-frequency measurement, light weight and so on [2].

The basic principle of photonic MFM systems is to map the frequency of an unknown microwave signal to a more easily measurable parameter, such as power and time delay. Systems based on frequency-to-power mapping [2]–[11] were the most common scheme and often offered advantages of low cost and simple structure. However, most frequency-to-power mapping systems could not

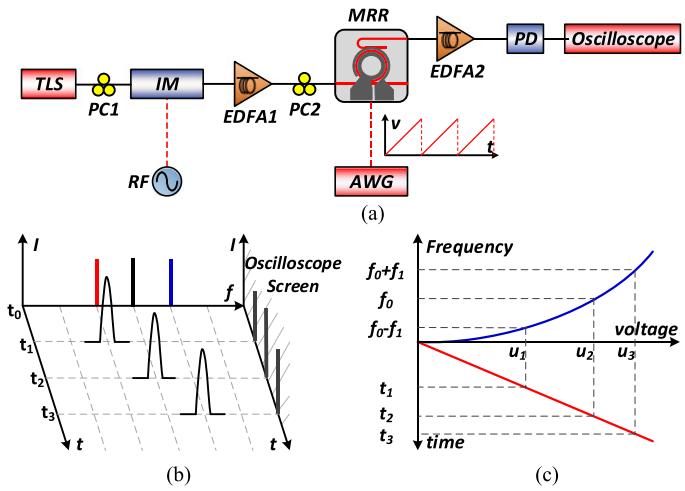

Fig. 1. (a) The schematic of the proposed MFM system. (b) The scanning filtering principle of the MRR. (c) The process of frequency-to-time mapping.

measure multi-frequency simultaneously [2]–[7], [9]–[11], making them less practical in the spectrally cluttered environment; or the input power needed to remain constant to match the amplitude comparison function (ACF) [4], [9]–[11]. By contrast, systems relying on frequency-to-time mapping [12]–[15] were usually qualified for multi-frequency measurements and the measurement accuracy was independent on the input power. In [12], time delay was generated by utilizing dispersion effect. However, its accuracy and resolution was unsatisfactory and the use of high-speed photodetector made the system expensive. In [13], a scanning receiver based on frequency shifting recirculating delay line and stimulated Brillouin scattering was proposed. However, the system latency was dependent on the number of circulation and the use of long single-mode fiber made system bulky. In [15], the laser should be continuously and linearly tuned and the performance was limited by the sweeping rate of the laser.

In this letter, a simplified photonic MFM system with a wide measurement range and a multi-frequency measurement ability is presented. A high-Q MRR, driven by a sawtooth voltage signal, serves as a periodic bandpass scanning filter. By scanning filtering, unknown frequency information is mapped into time interval and unknown frequencies can be derived using the frequency-to-time mapping function. A measurement range of 25 GHz, with an error of $\pm$510 MHz is achieved. The capability of multi-frequency measurement has been verified, with a resolution of 5 GHz. Meanwhile, the measurement does not rely on input power (both optical carrier and RF signal). Thus, the system can survive in cluttered microwave environment.

2. Principle and Structure

Fig. 1(a) shows the schematic diagram of the proposed MFM system based on MRR. The continuous-wave (CW) light carrier generated by a tunable laser (TLS) is launched into an intensity modulator (IM), modulated by the unknown microwave signal. Assuming that the unknown microwave signal has a single tone. After modulation (i.e., linear modulation), there are three frequency components in the signal, i.e., f_0 and $f_0 \pm f_1$. Here, f_0 is the frequency of CW light and f_1 is the frequency of input microwave signal. Two polarization controllers (PC1, 2) are placed before the IM and the MRR to optimize the polarization state of the incident light. Two erbium doped fiber amplifiers (EDFA1, 2) are placed before and after the MRR to compensate the link loss, respectively. The output from the drop-port of MRR is detected by a low-speed PD (BW: 200 MHz) and the photocurrent is observed with an oscilloscope.

We select one of the resonant peaks of the MRR, with a relatively narrow 3 dB bandwidth and a high extinction ratio as the narrowband filter. When a sawtooth voltage signal is applied on the

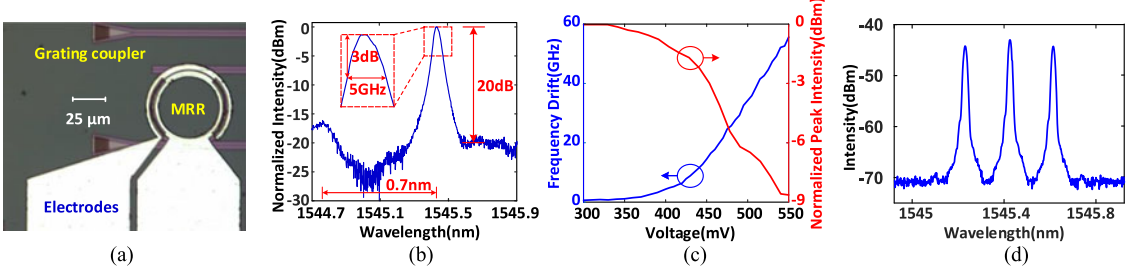

Fig. 2. (a) Microscope image of the MRR. (b) The normalized transmission spectrum of the selected region of the MRR. (c) The frequency drift and peak intensity attenuation when applying DC voltage signal. (d) Measured optical spectrum of IM output.

electrodes of the MRR, the resonant peak will be blue shifted periodically, revealing a periodic scanning filter. Fig. 1(b) illustrates the scanning filtering process in a single period. As the applied voltage increases gradually, the filter peak will drift toward high frequency. At different time of t_1, t_2 and t_3, the frequency components of $f_0 - f_1$, f_0 and $f_0 + f_1$ are selected to pass through the filter, respectively. Thus three intensity peaks will show up on the oscilloscope, respectively. Therefore, frequency components are mapped into time sequences. The frequency-to-time mapping is illustrated in Fig. 1(c), including two parts, i.e., frequency-to-voltage and voltage-to-time. In a single cycle, voltage-to-time mapping is a linear process and can be expressed as

$$u = at + b. \tag{1}$$

Here a and b are constants and determined by the properties of applied sawtooth voltage signal. The frequency-to-voltage function, expressed as $f(u)$, represents the relationship between the central frequency of the filter and voltage applied on the MRR. Obviously, input frequency f_1 is given by

$$f_1 = f(u_2) - f(u_1). \tag{2}$$

Combining (1) and (2), the frequency-to-time mapping function can be rewritten as

$$f_1(t) = f\left(at_2 + b\right) - f\left(at_1 + b\right). \tag{3}$$

Note that the function relationship $f(u)$ is dependent on the electrical characteristic of individual MRR in practical use, and should be measured and fitted in advance.

3. Experiments and Results

3.1 Microring Resonator and Modulator

The MRR is designed and fabricated on the silicon-on-insulator (SOI) wafer with a 220-nm-thick top silicon layer and a 2-μm-thick buried oxide layer. The microscope image of the MRR is shown in Fig. 2(a), consisting of two bus waveguides and one ring waveguide. Both the width of bus waveguides and ring waveguide are 500 nm and the gap between them is 330 nm. The radius of the ring is designed to be 59.88 μm. The ring waveguide is doped to form the p-i-n junction. Finally, aluminum is deposited to form electrodes. We employ plasma dispersion effect to tune the spectral response shift. More detailed fabrication process and related techniques can be found in Ref. [16]. Vertical grating couplers are employed to coupling the light between fiber and chip. The total loss of the chip is 18 dB, including 2-dB transmission loss and 16-dB coupling loss.

Fig. 2(b) shows the normalized transmission spectrum of the selected narrowband filter of MRR without voltage applied. The resonant wavelength is located at 1545.426 nm with a 3 dB bandwidth of 0.04 nm (about 5 GHz). The 3 dB bandwidth is of importance, since it determines the lower limit and the frequency resolution of measurement. The filter has a high extinction ratio (ER) of

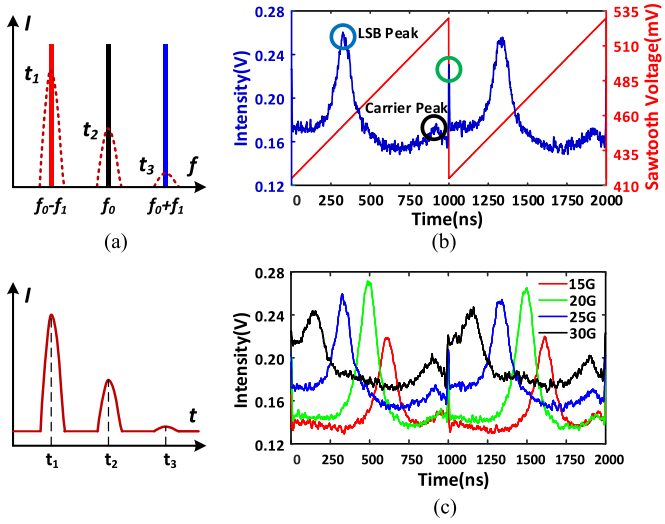

Fig. 3. (a) The expected filtering process and oscilloscope waveform due to filter peak attenuation. (b) The typical single frequency measurement waveform (blue curve, 25 GHz) and corresponding sawtooth voltage signal (red curve). (c) Measured waveforms on the oscilloscope of different single frequency signals.

20 dB. The suppression band in the lower wavelength side is more than 0.64 nm (about 80 GHz), indicating that the system is potential to achieve MFM up to 40 GHz.

Fig. 2(c) shows the filter response variation when different DC voltage signal is applied on the MRR. The blue curve shows the relationship between resonant frequency and voltage, apparently a nonlinear and monotonic process. The resonant frequency changes obviously only when the voltage is more than 300 mV. $f(u)$ is obtained by fitting the curve with high order polynomial. The red curve shows the filter peak decreases significantly when the voltage is higher than 400 mV. The decline may make the high frequency sideband high loss, resulting in failure of distinguishing the effective intensity from the noise. We have also tested the performance of the IM, as shown in Fig. 2(d). Here, the optical carrier is set at 1545.426 nm and input microwave frequency is set at 25 GHz. There are obviously three frequency components, i.e., carrier and first-order sidebands.

3.2 Microwave Frequency Measurement

Proof-of-concept experiments have been carried out based on the set up shown in Fig. 1(a). Preliminary experiment shows that only two intensity peaks can be observed on the oscilloscope in a single scanning cycle, corresponding to lower sideband and carrier, as illustrated in Fig. 3(a). Since the peak of the filter will experience significant attenuation when driven by a high voltage (i.e., at high frequency region), the high frequency sideband could not be measured effectively with the oscilloscope. Even so, two observed intensity peaks offer us enough information to estimate and retrieve the unknown frequency.

Based on the preliminary experiment, we optimize the parameters of all experiment setup, i.e., sawtooth voltage range, repetition rate of sawtooth signal and optical carrier wavelength. The TLS generates a CW with an output power of 10 dBm at the wavelength of 1545.1 nm, about 40.75 GHz (i.e., 0.326 nm) away from the selected resonant peak. The sawtooth voltage, generated by a low-speed arbitrary waveform generator (AWG), is set with a repetition rate of 1 MHz and a voltage range from 415 mV to 530 mV, shown in Fig. 3(b) (red curve). In this voltage range, the filter has a distinct frequency shift and only the lower sideband and carrier are scanned so that the scanning period is fully utilized, thus increasing the resolution of waveform.

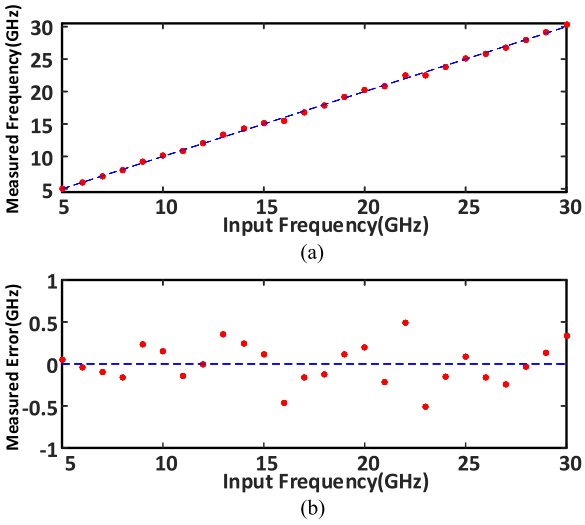

Fig. 4. (a) Frequency estimation from 5 GHz to 30 GHz. (b) Measurement errors for different frequency microwave signals.

When the IM is modulated by a single tone of 25 GHz, the measured waveform on the oscilloscope is shown in blue curve of Fig. 3(b). We observe a period of 1000 ns, consistent with that of the sawtooth voltage signal. Meanwhile, we observe two significant intensity peaks in one scanning period, marked with blue circle and black cycle, corresponding to lower sideband and optical carrier, respectively. Due to the high loss of filter peak when applying large voltage, the second intensity peak is much lower than the first one. Besides, a sharp pulse is observed at the voltage jump point, marked with green circle in Fig. 3(b). The sharp pulse is formed due to rapidly reverse filtering of MRR (intensity peaks are too close to each other), thanks to the steep falling edge of the sawtooth voltage. This sharp pulse is helpful to define the baseline and synchronization between input sawtooth signal and output intensity waveform, ensuring the measurement accuracy when the frequency-to-time mapping is nonlinear.

In order to evaluate the measurement performance of the proposed MFM system, we tune the microwave frequency from 5 GHz to 30 GHz with a step of 1 GHz. Fig. 3(c) shows several typical intensity waveforms in two scanning periods when input microwave frequency is set at 15 GHz, 20 GHz, 25 GHz and 30 GHz, respectively. We notice that time interval between the power peaks of lower sideband and optical carrier increases monotonically as the frequency of microwave signals increases. Note that the power ratio between LSB peak and carrier peak varies non-monotonically with frequency, which is not consistent with Fig. 2(c). This inconsistency is due to the performance of the IM. We found that when the input microwave frequency is higher than 20 GHz, the sideband intensity of output signal of the modulator begins to fall. Even so, it does not affect the measurement accuracy. The time appearance of intensity peak corresponding to carrier may drift a little in different frequency cases, indicating that the spectral response of the MRR has experienced unexpected drift. This drift is due to environmental temperature perturbation and certainly causes measurement error.

The 3 dB bandwidth of filter determines the lower limit for effective frequency measurement, which is 5 GHz. Hence, we investigate the measurement error by scanning the microwave frequency starting from 5 GHz. The maximum measurable frequency is 30 GHz, limited by the bandwidth of our microwave signal source.

Since we have obtained the intensity-time waveforms as illustrated in Fig. 3(c), the input microwave frequency can be calculated by measuring the time interval between the two intensity peaks and using (3). Fig. 4(a) shows the measurement results when scanning the input microwave frequency from 5 GHz to 30 GHz. Excellent agreement between the estimation values and the

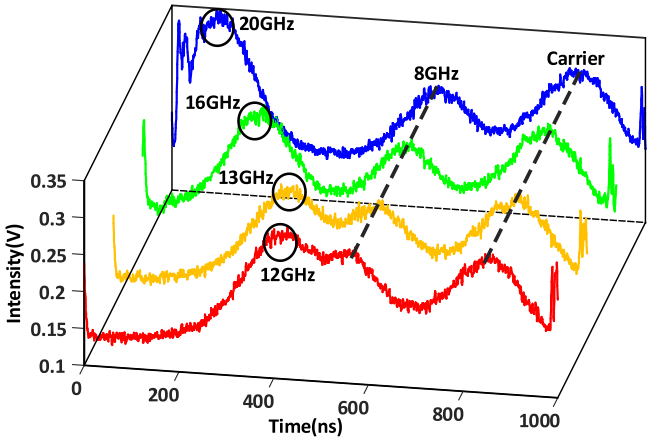

Fig. 5. Intensity-time waveforms on the oscilloscope of multi-frequency signals.

Table 1
Performance Comparison of Microwave Multi-Frequency Measurement Systems

Solutions	Range (GHz)	Error (MHz)	Resolution (GHz)	Integration	Nonlinear Optics
[8]	9–38	±1	0.05	Yes	Yes
[12]	15–45	±1560	12.5	No	No
[13]	0.1–20	200	0.25	No	Yes
[15]	1–15	90	0.2	No	No
This work	5–30	±510	5	Yes	No

input values can be seen. The measurement error is within ±510 MHz for different frequency microwave signals, as illustrated in Fig. 4(b). As mentioned above, the measurement error is induced by the 3 dB bandwidth of the filter, the nonlinearity of frequency-to-time mapping function and environmental temperature perturbation.

To verify the capability of multiple frequency measurement, two microwave signals with different frequencies are mixed (RF combiner, GTPD-COMB50G from Jitaitech) and loaded into the IM simultaneously. Meanwhile, to make the intensity peak corresponding to carrier more distinguishable, the wavelength of TLS is adjusted to 1545.181 nm, about 30.625 GHz shifted from the resonant wavelength of filter. In addition, the sawtooth voltage is set from 424 mV to 507 mV. Fig. 5 shows the measured results for the mixed frequency cases of 8 GHz and 12 GHz, 8 GHz and 13 GHz, 8 GHz and 16 GHz, as well as 8 GHz and 20 GHz. The central and right peaks represent input microwave of 8 GHz and optical carrier respectively and their appearance time is stable. One can see the multiple frequencies can be distinguished easily for cases of 8 GHz mixed with 20 GHz, 8 GHz mixed with 16 GHz, and 8 GHz mixed with 13 GHz. However, when the frequency difference between two signals is lower than 5 GHz, i.e., for the case of 8 GHz and 12 GHz, the measured intensity peaks are hardly to be distinguished from each other. This indicates that the multiple frequency resolution is about 5 GHz, limited by the 3 dB bandwidth of the selected filter.

Table 1 shows the performance comparison of existing microwave multi-frequency measurement systems. It can be seen that the proposed MFM system has a compact size thanks to the use of silicon photonics chip and a relatively wide measurement range. Meanwhile, our scheme offers

a simple structure and low cost solution, since no high-speed device is needed in the measurement process expect the intensity modulator. Besides, the avoidance of nonlinear effect such as stimulated Brillouin scattering makes the system more energy-efficient. The system can be further improved by using an MRR with better performance. MRRs with higher quality factor [17] and higher tuning speed [18] have been reported. The higher Q-factor guarantees improved accuracy, lower measurement limit and multi-frequency resolution, while high tuning speed reduces system latency. Meanwhile, the implementation of monolithic integrated microwave photonics (MWP) systems [19], [20] has been reported, which manifests that the proposed MFM system has potential to achieve monolithic integration thanks to its simple structure.

4. Conclusion

In conclusion, we have presented a frequency-to-time mapping MFM system that enables measurement of multiple frequency signals in a relatively wideband. Frequency estimation in a range of 5–30 GHz with a measurement error under $\pm$510 MHz is achieved. Besides, the resolution is about 5 GHz for multi-frequency measurement. Our scheme offers a simple structure, low cost solution, capability of multiple frequency measurement and potential of chip-integration.

References

[1] X. Zou, B. Lu, W. Pan, L. Yan, A. Stöhr, and J. Yao, "Photonics for microwave measurements," *Laser Photon. Rev.*, vol. 10, no. 5, pp. 711–734, 2016.

[2] J. Jiang *et al.*, "Photonic-assisted microwave frequency measurement system based on a silicon ORR," *Opt. Commun.*, vol. 382, pp. 366–370, 2017.

[3] D. Marpaung, "On-chip photonic-assisted instantaneous microwave frequency measurement system," *IEEE Photon. Technol. Lett.*, vol. 25, no. 9, pp. 837–840, May 2013.

[4] N. Sarkhosh, H. Emami, L. Bui, and A. Mitchell, "Reduced cost photonic instantaneous frequency measurement system," *IEEE Photon. Technol. Lett.*, vol. 20, no. 18, pp. 1521–1523, Sep. 2008.

[5] M. Burla, X. Wang, M. Li, L. Chrostowski, and J. Azana, "Wideband dynamic microwave frequency identification system using a low-power ultracompact silicon photonic chip," *Nature Commun.*, vol. 7, Sep. 2016, Art. no. 13004.

[6] L. A. Bui and A. Mitchell, "Amplitude independent instantaneous frequency measurement using all optical technique," *Opt. Exp.*, vol. 21, no. 24, pp. 29601–29611, Dec. 2013.

[7] J. S. Fandino and P. Munoz, "Photonics-based microwave frequency measurement using a double-sideband suppressed-carrier modulation and an InP integrated ring-assisted Mach-Zehnder interferometer filter," *Opt. Lett.*, vol. 38, no. 21, pp. 4316–4319, Nov. 2013.

[8] H. Jiang *et al.*, "Wide-range, high-precision multiple microwave frequency measurement using a chip-based photonic Brillouin filter," *Optica*, vol. 3, no. 1, pp. 30–34, 2016.

[9] M. Pagani *et al.*, "Low-error and broadband microwave frequency measurement in a silicon chip," *Optica*, vol. 2, no. 8, pp. 751–756, 2015.

[10] L. Liu *et al.*, "Photonic measurement of microwave frequency using a silicon microdisk resonator," *Opt. Commun.*, vol. 335, pp. 266–270, 2015.

[11] M. Pagani, K. Vu, D.-Y. Choi, S. J. Madden, B. J. Eggleton, and D. Marpaung, "Instantaneous microwave frequency measurement using four-wave mixing in a chalcogenide chip," *Opt. Commun.*, vol. 373, pp. 100–104, 2016.

[12] L. Nguyen, "Microwave photonic technique for frequency measurement of simultaneous signals," *IEEE Photon. Technol. Lett.*, vol. 21, no. 10, pp. 642–644, 2009.

[13] T. A. Nguyen, E. H. Chan, and R. A. Minasian, "Instantaneous high-resolution multiple-frequency measurement system based on frequency-to-time mapping technique," *Opt. Lett.*, vol. 39, no. 8, pp. 2419–2422, Apr. 2014.

[14] S. T. Winnall and A. C. Lindsay, "A Fabry-Perot scanning receiver for microwave signal processing," *IEEE Trans. Microw. Theory Tech.*, vol. 47, no. 7, pp. 1385–1390, Jul. 1999.

[15] C. Ye, H. Fu, K. Zhu, and S. He, "All-optical approach to microwave frequency measurement with large spectral range and high accuracy," *IEEE Photon. Technol. Lett.*, vol. 24, no. 7, pp. 614–616, Apr. 2012.

[16] L. Liu, M. He, and J. Dong, "Compact continuously tunable microwave photonic filters based on cascaded silicon microring resonators," *Opt. Commun.*, vol. 363, pp. 128–133, 2016.

[17] M.-C. Tien, J. F. Bauters, M. J. R. Heck, D. T. Spencer, D. J. Blumenthal, and J. E. Bowers, "Ultra-high quality factor planar Si_3N_4 ring resonators on Si substrates," *Opt. Exp.*, vol. 19, no. 14, pp. 13551–13556, Jul. 2011.

[18] X. Xiao *et al.*, "44-Gb/s silicon microring modulators based on zigzag PN junctions," *IEEE Photon. Technol. Lett.*, vol. 24, no. 19, pp. 1712–1714, Oct. 2012.

[19] J. S. Fandiño, P. Muñoz, D. Doménech, and J. Capmany, "A monolithic integrated photonic microwave filter," *Nature Photon.*, vol. 11, no. 2, pp. 124–129, 2016.

[20] W. Zhang and J. Yao, "A silicon photonic integrated frequency-tunable microwave photonic bandpass filter," in *Proc. 2017 Int. Top. Meeting Microw. Photon.*, 2017, pp. 1–4.